SpringerWienNewYork

Thomas P. Naidich, Henri M. Duvernoy, Bradley N. Delman,
A. Gregory Sorensen, Spyros S. Kollias and E. Mark Haacke

Duvernoy's Atlas of the Human Brain Stem and Cerebellum

High-Field MRI: Surface Anatomy, Internal Structure, Vascularization and 3D Sectional Anatomy

With contributions by

T. Benner	W. Boonn	F. Cattin
P. Choi	J. Delgado	P. Hof
M. Law	W. Lin	J. Linn
Y. Lui	A. Macedo	E. Manova
M. Sasaki	M. Schwartz	E. Shibata
A. Tai	C. Tang	D. Wolfe
C. Yeo	I. Yousry	T. Yousry

Drawings by Jean-Louis Vannson

SpringerWienNewYork

Thomas P. Naidich, M. D.
Professor of Radiology and Neurosurgery
Irving and Dorothy Regenstreif Research Professor of Neuroscience (Neuroimaging)
Director of Neuroradiology, Mount Sinai School of Medicine of New York University, New York, NY, USA

Henri M. Duvernoy, M. D.
Anatomist, emeritus
Laboratoire d'Anatomie, Faculté de Médecine et de Pharmacie, Université de Franche-Comté, Besançon, France

Bradley N. Delman, M. D.
Associate Professor of Radiology
Department of Radiology, Mount Sinai School of Medicine of New York University, New York, NY, USA

A. Gregory Sorensen, M. D.
Associate Professor in Radiology at Harvard Medical School
Co-Director: Athinoula A. Martinos Center for Biomedical Imaging,
Harvard Medical School, Boston, MA, USA

Spyros S. Kollias, Prof. Dr. med.
Professor of Neuroradiology, Vice-Chairman of the Institute of Neuroradiology
University Hospital of Zurich, Switzerland

E. Mark Haacke, Ph. D.
Professor of Radiology, Director: MR Research Facility
Wayne State University, Detroit, MI, USA

Printed in Austria

SpringerWienNewYork is part of
Springer Science + Business Media
springer.at

Illustrations: Figures 2.2, 2.3, 2.7, 3.6, 4.17–4.19 redrawn by Stefan Kindel
Typesetting and Printing: Holzhausen Druck und Medien GmbH, 1140 Wien, Austria

Printed on acid-free and chlorine-free bleached paper
SPIN: 12061198

With numerous (partly coloured) Figures

Library of Congress Control Number: 2007934675

ISBN 978-3-211-73970-9 SpringerWienNewYork

DEDICATIONS

We dedicate this text to those who gave of themselves to train us and to the trainees who have entrusted us with years of their lives for what we now pass on to them.

Successful completion of this project depended upon real physical and emotional support for us from colleagues, families and friends. We gratefully thank them for their encouragement during the endless hours needed to bring this material together.

Henri M. Duvernoy:	To my family – Odile, Charles and David Duvernoy
Thomas P. Naidich:	To my wife Michele, my daughter Sandra, my brother James, and the loving memory of my parents James and Rose Naidich. May this meet your expectations.
Bradley N. Delman:	To my wife Allissa and young daughter Maya, who lovingly endured my absence through many late nights and even later mornings
A. Gregory Sorensen:	To my family: Kristiina, Rachel, Caroline and Samuel
Spyros S. Kollias:	To the next generation of Neuroradiologists
E. Mark Haacke:	To all those students and faculty who have helped in our quest to take research concepts and put them into clinical practice.

ACKNOWLEDGMENTS

The authors thank the Manhattan HIV and Manhattan Hepatology Brain Banks (R24MH59724) for providing normal control brain stems for 9.4 Tesla imaging.

We deeply thank Dr. Burton P. Drayer, The Dr. Charles M. and Marilyn Newman Professor of Radiology, Chairman of Radiology and President of the Mount Sinai Hospital, Dr. Zvi Lefkovitz, Vice-Chairman of Radiology, and Dr. Zahi Fayad, Director of the Imaging Science Laboratories of the Mount Sinai Medical Center, for their strong support of this project. We give a warm and special thanks to Ronit Gilad, M.D. for her research assistance with Section IX – Cranial Nerves, and acknowledge our very large debt to Drs. Daniel Perl, Susan Morgello, and George Kleinmann of the Section of Neuropathology, Mount Sinai Medical Center for sharing their knowledge of brain stem anatomy.

We also thank Juan Gilberto S. Aguinaldo M. D., Daniel D. Samber P. E. and all of the staff of the Imaging Science Laboratories for their technical help in obtaining the 9.4 Tesla MR images. We gratefully acknowledge the imaging assistance of John C. Gentile R.T., Hanna Oltarzewska R.T., and Frank M. Macaluso R.T., B. S. for their assistance with the 3 Tesla images.

The authors also wish to acknowledge the help of those "who have directly participated in this work":
Mr. J. L. Vannson, Mrs. J. Euvrard, Mrs. A. Barthelet, Mrs. F. Gillet, Mrs. Asya Volberg, and Ms. Elba Colman.

We greatly appreciate the expertise of Mr. Wolfgang Dollhäubl of Springer Wien New York. We would like to thank him for the very real help he gave us in laying out and producing this volume, for the elegant technical solutions he provided to tricky problems, and for the grace and patience with which he guided us toward the finished work.

CONTENTS

LIST OF CONTRIBUTORS

Thomas P. Naidich, M. D.
Professor of Radiology and Neurosurgery
Irving and Dorothy Regenstreif Research Prof.
of Neuroscience (Neuroimaging)
Director of Neuroradiology
Mount Sinai School of Medicine of New York University
One Gustave L. Levy Place
New York, NY 10029, USA
E-mail: thomas.naidich@mountsinai.org

Henri M. Duvernoy, Prof. Dr. med.
Faculté de Médecine et de Pharmacie
Université de Franche-Comté Besançon
12 chemin des Relancons, 25000 Besançon, France
E-mail: henri.duvernoy@wanadoo.fr

Bradley N. Delman, M. D.
Associate Professor of Radiology
Department of Radiology
Mount Sinai School of Medicine of New York University
One Gustave L. Levy Place
New York, NY 10029, USA
E-mail: bradley.delman@mountsinai.org

A. Gregory Sorensen, M. D.
Associate Professor in Radiology at Harvard Medical School, Co-Director: Athinoula A. Martinos Center for Biomedical Imaging
149 Thirteenth Street, Suite 2301
Charlestown, MA 02129, USA
E-mail: sorensen@nmr.mgh.harvard.edu

Spyros S. Kollias, Prof. Dr. med.
Professor of Neuroradiology
Vice Chairman Institute of Neuroradiology
Chief of Magnetic Resonance Imaging
University Hospital of Zurich
Frauenklinikstr. 10
8091 Zurich, Switzerland
E-mail: kollias@dmr.usz.ch

E. Mark Haacke, Ph. D.
Professor of Radiology
Director: MR Research Facility
Wayne State University
HUM-MR Research
G0301 Radiology
3990 John R. Road
Detroit, MI 48201, USA
E-mail: nmrimaging@aol.com

Thomas Benner, Ph. D.
Instructor in Radiology at Harvard Medical School
Athinoula A. Martinos Center for
Biomedical Imaging
149 Thirteenth Street, Suite 2301
Charlestown, MA 02129, USA
E-mail: benner@nmr.mgh.harvard.edu

William W. Boonn, M. D.
Associate Director of Clinical Imaging Informatics
Department of Radiology
Hospital of the University of Pennsylvania
3400 Spruce Street
Philadelphia, PA 19104, USA
E-mail : bill@medicalpocketpc.com

Françoise Cattin, M. D.
Service de Neuroradiologie
Centre Hospitalier Universitaire J. Minjoz
Besançon, France
E-mail: fcattin@chu-besançon.fr

Paul S. Choi, M. D.
Radiologist, East River Medical Imaging
519 East 72nd Street
New York, NY 10021, USA
E-mail: pchoi@eastriverimaging.com

Josser E. Delgado-Almandoz, M. D.
Department of Radiology, Founders 216
Harvard University School of Medicine
Massachusetts General Hospital
55 Fruit Street
Boston, MA 02114, USA
E-mail: jdelgadoalmandoz@partners.org

Patrick R. Hof, M. D.
Irving and Dorothy Regenstreif Research
Professor of Neuroscience (Neurobiology)
Chairman, Department of Neuroscience
Mount Sinai School of Medicine of New York University
One Gustave L. Levy Place
New York, NY 10029, USA
E-mail: patrick.hof@mssm.edu

Meng Law, M. D., F. R. A. C. R.
Associate Professor of Radiology and Neurosurgery
Department of Radiology
Mount Sinai School of Medicine of New York University
One Gustave L. Levy Place
New York, NY 10029, USA
E-mail: meng.law@mountsinai.org

Wen Lin, M. D.
Mount Sinai School of Medicine of New York University
One Gustave L. Levy Place
New York, NY 10029, USA
E-mail: wen.lin@mssm.edu

Jennifer Linn, Dr. med.
Department of Neuroradiology
University Hospital Munich
Marchioninistr. 15
81377 Munich, Germany
E-mail: jennifer.linn@med.uni-muenchen.de

Yvonne W. Lui, M. D.
Assistant Professor of Radiology
Department of Radiology, Albert Einstein College
of Medicine of Yeshiva University
Montefiore Medical Center
111 East 210th Street
Bronx, NY 10467, USA
E-mail: ylui@montefiore.org

Aisha A. Macedo, M. D.
Department of Ophthalmology
Mount Sinai Medical Center of New York University
One Gustave L. Levy Place
New York, NY 10029, USA
E-mail: aisha.macedo@mssm.edu

Elena Manova, M. S.
Graduate Research Assistant
Biomedical Engineering Department and
MR Research Facility
Wayne State University
818 West Hancock
Detroit, MI 48201, USA
E-mail: nmrimaging@aol.com

Michael B. Schwartz, M. D.
Department of Radiology
Weill-Cornell School of Medicine
525 East 70th Street
New York, NY 10021, USA
E-mail: michael.schwartz01@mssm.edu

Eri Shibata, M. D.
Postdoctoral Fellow
Department of Neuropsychiatry
Iwate Medical University School of Medicine
19-1 Uchimaru, Morioka 020-8505, Japan
E-mail: eshibata@iwate-med.ac.jp

Makoto Sasaki, M. D.
Assistant Professor of Radiology
Iwate Medical University School of Medicine
19-1 Uchimaru, Morioka 020-8505, Japan
E-mail: masasaki@iwate-med.ac.jp

Angela W. Tai, M. D.
Department of Radiology
Brigham and Women's Hospital
75 Francis Street
Boston, MA 02115, USA
E-mail: awtai@partners.org

David E. Wolfe, M. D.
Associate Professor of Pathology
Mount Sinai School of Medicine of New York University
One Gustave L. Levy Place
New York, NY 10029, USA

Christopher H. Yeo, Ph. D.
Professor of Behavioural Neuroscience
Department of Anatomy and Developmental Biology
University College London
London, WC1E 6BT, UK
E-mail: c.yeo@ucl.ac.uk

Cheuk Ying Tang, Ph. D.
Assistant Professor of Radiology
Department of Radiology and Imaging
Science Laboratory
Mount Sinai School of Medicine of New York University
One Gustave L. Levy Place
New York, NY 10029, USA
E-mail: cheuk.tang@mssm.edu

Indra Yousry, Dr. med. Privat Dozent
Department of Neuroradiology
Klinikum Grosshadern
Ludwig Maximilian Universität
81377 Munich, Germany
E-mail: indra.yousry@med.uni-muenchen.de

Tarek A. Yousry, Dr. med. habil, F. R. C. R.
Professor of Neuroradiology
Head, Lysholm Department of Neuroradiology
The National Hospital for Neurology
and Neurosurgery
Institute of Neurology
8-11 Queen Square, London WC1N 3BG, UK
E-mail: t.yousry@ion.ucl.ac.uk

INTRODUCTION

This study of the brain stem and cerebellum builds upon the prior publications [1–491] and presentations [A1–A9] of many investigators, and incorporates portions of our own work on the encephalon (cerebral hemispheres and diencephalon) [125], the brain stem and cerebellum [121, 123, 128], and brain vascularity [120, 122]. Large new sections have been added to reflect the great advances in anatomic MR imaging since the first edition [121]. All sagittal images have been re-oriented and relabelled to conform to standard MR display. As in the first edition, each section is organized so that early images teach the overview, while later images provide the detailed knowledge required for understanding serial anatomic and MR sections and their clinical utility.

Following a brief survey of the methods used:

Section I describes the surface anatomy of the brain stem and cerebellum as well as their location in the posterior cranial fossa.

Sections II–IV describe the internal structure of the brain stem and cerebellum and then summarize their function, to introduce the roles of individual nuclei and fasciculi within and traversing the brain stem and cerebellum.

Section V addresses the anatomy of the mesencephalic-diencephalic junction.

Section VI depicts the vascular network of the brain stem in detail and summarizes the results of the authors' prior research on both the superficial blood vessels and the intrinsic vascular territories of the brain stem [120, 122, 307, 308]. The description of cerebellar vascularization derives predominantly from the literature rather than personal investigation.

Section VII depicts the intrinsic vascular territories of the brain stem, and illustrates these with clinical images of human brain stem infarctions.

Section VIII presents near-histologic sections of the brain stem in three orthogonal planes, obtained using 9.4 Tesla magnetic resonance microscopy (MRM) of formalin-fixed human cadaver specimens. Although some details depicted in these sections are beyond present clinical imaging, we believe that future advances in MR and computer technology will render them clinically useful in the coming years.

Section IX illustrates the intra-axial and cisternal courses of the cranial nerves, to show their complete trajectories from the nuclei of origin to the exit foramina in the skull base.

Section X illustrates advanced MR techniques for depicting neuromelanin, brain iron, and fiber tract orientation, enhancing our understanding of brain stem anatomy.

Section XI correlates serial 2–4 mm thick sections of the brain in axial, coronal and sagittal planes with clinical 3 Tesla T1- and T2-weighted MR images obtained with a 32-channel surface array head coil. All the clinical MR images are of the same volunteer, studied in two sequential sessions, so the anatomic relationships shown may be correlated directly with each other and with the anatomic specimens in all three orthogonal planes. Due to individual variation in head shape (brachycephalic vs. dolichocephalic), some structures shown together on the anatomic sections are seen to lie in adjacent MR sections in vivo, and vice versa. Not all of the strucures indicated on the anatomic images are yet demonstrable on the clinical MR images. However, the locations of these important structures may be inferred on MR images from their known anatomic relationships to other, larger structures. As with the MR microscopic images, these smaller structures will become increasingly easier to display – and increasingly important to appreciate – in the near future.

This text uses the common non-Latin anatomical terminology. Latin terms are used only where common usage has not supplanted the original Latin nomenclature.

METHODS

Differing methods were used to study the surfaces of the brain stem and cerebellum, the structures and vascular networks of these regions, specific features such as neuromelanin, and the serial three-dimensional sections.

The surfaces of the brain stem and cerebellum

Thirty human encephala were examined following fixation in a 10% formalin solution sufficiently voluminous to prevent their distortion. Both cerebral hemispheres were removed. What remained thus comprised the brain stem, cerebellum, and diencephalon. These structures were immersed in a 30% alcohol solution and then dissected under a stereoscopic microscope and photographed in distilled water to prevent degradation of the images by light reflections. So far as possible, each specimen was photographed in three oblique views to provide anatomic references for the specific section illustrated.

The structures and vascular network of the brain stem and cerebellum

The material and methods used in this study are derived from previous works [119, 120, 122, 123, 127, 128, 129, 130, 131]. Sixty brains were examined after having undergone two processes: intravascular injection with India ink and plastics, and Bodian's method of silver impregnation.

Intravascular injection (Capillary maps)

The brains were injected with 400 cm^3 of a solution containing India ink and 5% gelatin. After fixation, dehydration, immersion into toluene, and embedding in paraffin, the relevant portions were cut into serial thick sections (400 μm), which were then cleared in a Spalteholz solution (methylsalicylate and benzyl benzoate). Intravascular injection with low viscosity resin (Mercox) completed the previous study, and further defined the fine vascular network and its spatial organization. After injection, the perivascular tissue was removed and the vascular network was examined with a scanning electron microscope.

The complementary India ink and resin injection techniques provided a "map" of differences in capillary density across the brain stem. The density of injected capillaries varied sustantially from gray matter (higher capillary density) to white matter (lower capillary density) and even varied among different gray matter nuclei. These "capillary maps" enabled specific localization and identification of dense, highly vascular gray matter nuclei and the adjacent less dense, less well vascularized white matter tracts.

Bodian's method of silver impregnation

A specific advantage of the India ink injection technique is that it permits use of subsequent histological techniques, such as the Bodian silver impregnation technique, to confirm the anatomic analysis. Specifically, use of serial thick sections showing the vascular pattern and alternating thin silver-impregnated sections showing the anatomic structures, enabled us to characterize the patterns of vascularization of the gray matter of the brain stem and cerebellum. However, these methods provide only limited depiction of white matter, so only large fasciculi can be appreciated directly (e. g., corticospinal tracts, medial lemnisci, medial longitudinal fasciculi, and central tegmental tracts). The numerous smaller fasciculi of the brain stem (**seen on Figs. 2.7–2.22**) were localized only through their known relationships to the gray nuclei actually displayed.

The superficial blood vessels and brain stem vascular territories

The same India ink injection methods successfully display the overlapping arterial and venous networks of the superificial pial vasculature of the brain stem (**Figs. 6.1–6.36**). Using a stereoscopic microscope to examine

2–3 mm thick sections cleared by the Spalteholz technique, we could localize the points at which the arteries enter – and veins exit – the nervous tissue, and then trace the distribution of each vessel to map the intrinsic arterial and venous teritories of the whole brain stem (Figs 7.4–7.24) [122]. The vascular mapping proposed here may vary slightly from individual to individual. However, a less detailed examination of ten other brain stems appears to confirm the initial conclusions reported in this work

MR Microscopy (MRM) at 9.4 Tesla

Ten human cadaver brain stems were fixed in 15% formalin for two weeks, suspended in phosphate buffer, and then imaged in all three orthogonal planes with a Brüker 9.4 Tesla superconducting magnet (Brüker Analytik, Rheinstetten, Germany). The scanner used an 89 mm bore, a 35 mm bird cage coil, and intermediate-weighted pulse sequences: [Repetition time (TR): 1800–2500 msec, Echo time (TE): 20–30 msec, Slice thickness: 500 microns, Field of View: 20–35 mm, and Data matrix: 512 x 512 to 640 x 640 (interpolated to 1024 x 1024)]. This technique achieves images with an in-plane resolution of 30 to 68 microns. The narrow diameter of the bore and the coil often required the specimens to be trimmed or "halved" to fit within the scanner. The resultant intermediate-weighed MRM images were correlated with the injected specimens (capillary maps) (Figs. 2.7–2.22 and 6.38–6.51) and with standard atlases of neuroanatomy [4, 7, 15, 39, 78, 79, 99, 101, 106, 107, 109, 120, 122, 124, 125, 147, 155, 164, 167, 179, 231, 243, 294, 322a, 327, 328, 332, 335, 358, 370, 396, 423] to identify the structures depicted.

Serial images of the brain stem were then organized into a detailed atlas of the fiber tracts and nuclei of the brain stem in axial, sagittal and coronal planes (Figs. 8.1–8.147). Within each anatomic area (except the midbrain), all of the images displayed are from a single specimen, so the anatomic relationships among structures may be compared directly in all three orthogonal planes. Two different specimens were required to image the midbrain. Different specimens are illustrated for the different anatomic regions.

Advanced MR Imaging

Specific MR techniques have evolved to demonstrate neuromelanin (Figs. 10.1–10.3) [373, 394], susceptibility changes from parenchymal iron and intra-vasculature deoxyhemoglobin (Figs. 10.4–10.14) [177], and fiber tract orientation (Figs. 10.15–10.38) [28, 34, 146, 192, 217, 223, 275, 276, 293, 296, 297, 298, 299, 301,302, 303, 306, 316, 317, 345, 371, 407, 447, 453, 459] *in vivo*. These images are presented and correlated with both (i) sections of the whole head, and (ii) 3T images of formalin-fixed whole brains to illustrate the specific aspects of anatomy that they depict. The technical details of these techniques are given in the introduction to each of these sections.

Three-dimensional serial sections of the head

Three preparations, each including the brain stem, cerebellum, and diencephalon were cut into 2 to 4 mm thick sections by a circular-blade electric slicer.

The axial sections (Figs. 11.1–11.29) were obtained in the intercommissural plane of Schaltenbrand, which extends from the mid anterior commissure (AC) to the mid posterior commissure (PC) [1, 377, 378, 423, 424, 425]. This differs slightly from the standard bicommissural plane of Talairach, which is drawn from the top of the anterior commissure to the bottom of the posterior commissure [420, 421]. Coronal plane anatomic sections (Figs. 1.30–11.55) were obtained perpendicular to Schaltenbrand's intercommisural line. The sagittal sections (Figs. 11.56–11.70) were obtained parallel to the median plane.

Although the neuro-orbital plane recommended by Cabanis [69, 70] and the posterior commissure-obex (PC-O) plane of Tamraz [423–425] might have been better adapted to the sectional anatomy of the brain stem, we chose Schaltenbrand's intercommissural plane in order to build upon our previous studies of the sectional anatomy of the brain [125].

The principle of the three-dimensional serial sections is to gradually erode the preparation by sectioning it from inferior to superior for axial sections, from anterior to posterior for coronal sections, and from lateral to medial for sagittal sections. Each section then displays the anatomy of that section in relationship to the remaining portions of uneroded brain.

Each plate demonstrates the surface of the prepared section viewed "en face", plus diverse oblique views of the preparation to orient the viewer.

The serial sections of the eroded brain were correlated with anatomic sections of the head to show the brain *in situ*, and to show the relationship of the brain to the skull. The specific reference plane chosen for the head sections was the suborbito-meatal plane, which passes from the lower margins of the bony orbits to the centers of the external auditory canals. This external plane appears to correlate best with the internal intercommissural plane of Schaltenbrand.

Correlative T1- and T2-weighted clinical magnetic resonance images (MRI) were obtained in vivo at 3 Tesla (Siemens Trio, Erlangen, Germany), along the same reference planes parallel to and perpendicular to Schaltenbrand's intercommissural plane, utilizing a 32-channel surface array custom-built head coil (courtesy of Graham C. Wiggins Ph. D. and Larry L. Wald Ph. D.). These clinical images were then matched as closely as possible to the prepared anatomic specimens. The same volunteer was imaged for the axial, coronal and sagittal planes to enhance the value of correlations among the different planes. Because these lengthy MR sequences required two sessions to complete, the precise plane of section does vary slightly among images.

SECTION I

SURFACE ANATOMY OF THE BRAIN STEM AND CEREBELLUM

This chapter on the surface anatomy of the brain stem and cerebellum is divided into several portions:

A. General remarks on the encephalon
B. Surface of the brain stem
C. Surface of the cerebellum
D. Relationship between brain stem and cerebellum; emergence of the cranial nerves
E. The fourth ventricle
F. Lengths and angular relationships among these structures

A. General remarks

The encephalon comprises:

- The brain itself (prosencephalon) formed by the telencephalon (cerebral hemispheres),
- The diencephalon,
- The cerebellum, and
- The brain stem.

The brain is set in the anterior and middle cranial fossae, while the cerebellum and brain stem are located in the posterior cranial fossa. The anterior and middle cranial fossae are partially separated from the posterior fossa by the tentorium cerebelli, but communicate with the posterior fossa through the tentorial hiatus. The mesencephalon passes through this opening and joins the brain stem and cerebellum below with diencephalon and telencephalon above. **Figures 1.1–1.3** display the anatomic relationships among the different portions of the encephalon. The boundaries of the posterior cranial fossa are described in **Fig. 1.30**.

The brain stem is composed of 3 parts: in ascending order the medulla, the pons, and the mesencephalon.

The cerebellum is also composed of 3 parts: a median vermis and paired right and left cerebellar hemispheres.

The medulla, pons, and cerebellum together form the rhombencephalon, which encloses the fourth ventricle. The fourth ventricle is connected to the third ventricle through the cerebral aqueduct of Sylvius and to the subarachnoid spaces through the median foramen of Magendie and the paired lateral foramina of Luschka.

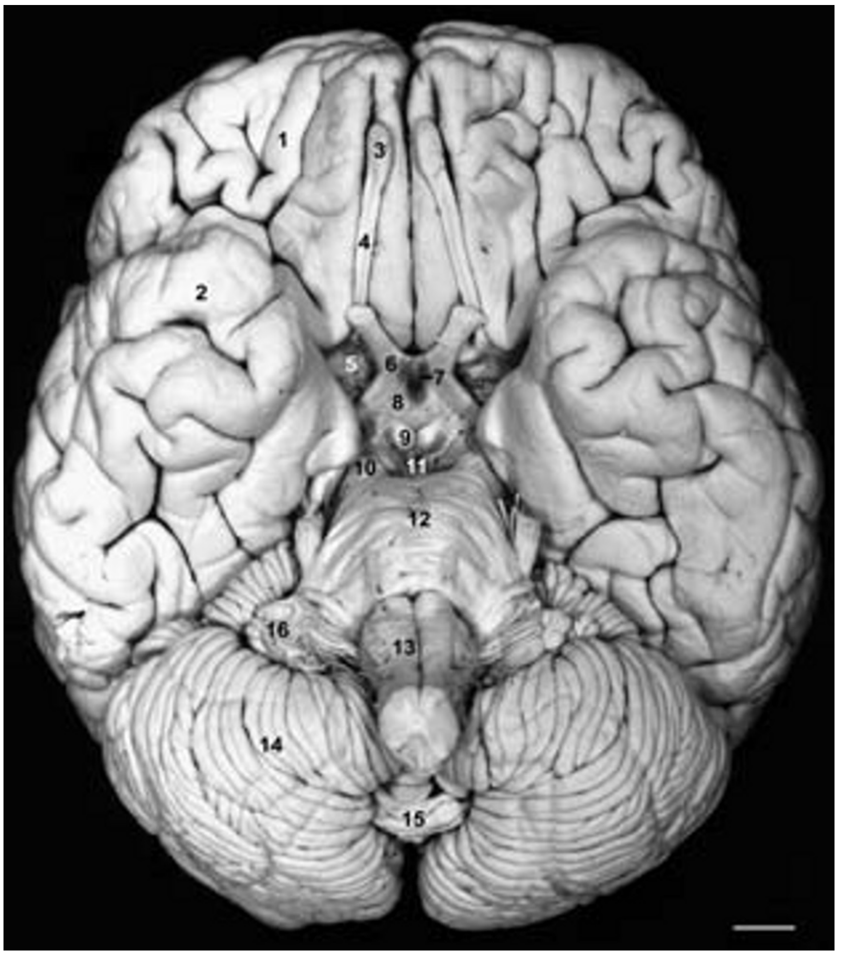

Fig. 1.1. The encephalon. Ventral aspect.
Bar: 10 mm

Cerebral hemisphere
1 Frontal (orbital) lobe
2 Temporal lobe
3 Olfactory bulb
4 Olfactory tract
5 Anterior perforated substance

Diencephalon
6 Optic chiasm
7 Hypophyseal stalk
8 Tuber cinereum
9 Mammillary body

Brain stem
10 Mesencephalon (crus cerebri)
11 Interpeduncular fossa
12 Pons
13 Medulla

Cerebellum
14 Cerebellar hemisphere
15 Vermis
16 Flocculus

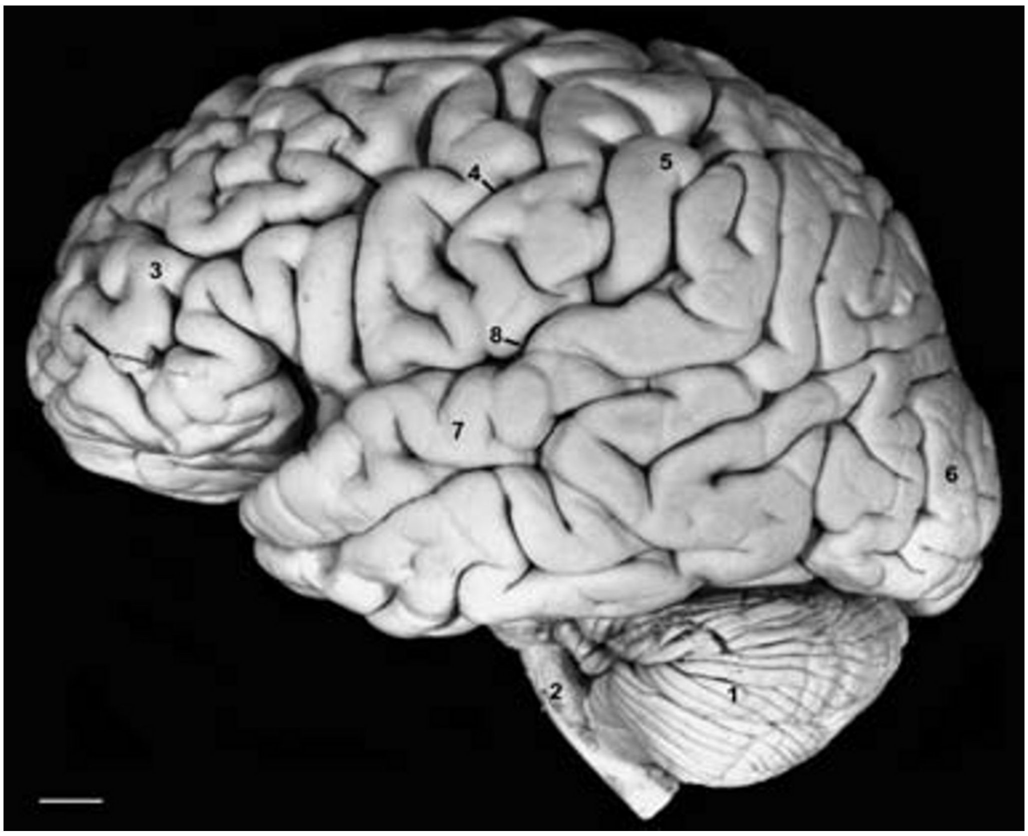

Fig. 1.2. The encephalon. Lateral aspect. Cerebral hemisphere.
Bar: 10 mm.

1 Cerebellar hemisphere
2 Brain stem
3 Frontal lobe
4 Central sulcus
5 Parietal lobe
6 Occipital lobe
7 Temporal lobe
8 Lateral (Sylvian) fissure

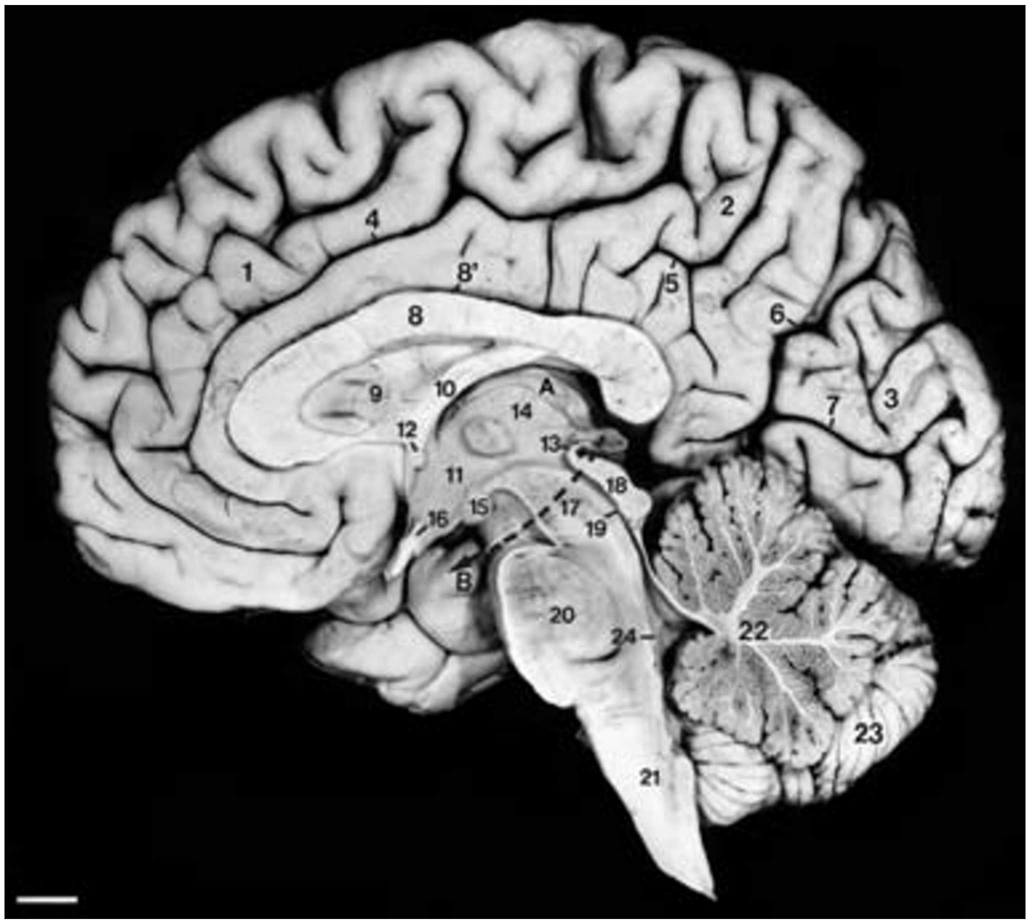

Fig. 1.3. The encephalon. Median section.
Bar: 10 mm.

Cerebral hemisphere (medial aspect)
1 Medial aspect of the frontal lobe
2 Medial aspect of the parietal lobe
3 Medial aspect of the occipital lobe
4 Cingulate sulcus
5 Subparietal sulcus
6 Parieto-occipital fissure
7 Calcarine sulcus
8 Corpus callosum
8′ Callosal sulcus
9 Septum pellucidum
10 Fornix

Diencephalon
11 Third ventricle
12 Anterior commissure
13 Posterior commissure
14 Thalamus
15 Mammillary body
16 Optic chiasm

Brain stem
17 Mesencephalon (crus cerebri)
18 Mesencephalon (tectum)
19 Cerebral aqueduct
20 Pons
21 Medulla

Cerebellum
22 Vermis
23 Medial aspect of the cerebellar hemisphere
24 Fourth ventricle

The median axis, composed of the brain stem and diencephalon, is partially covered by the bulk of the hemispheres during brain growth. Because the hemispheres adhere only partially to the diencephalon and mesencephalon, a transverse fissure still separates the fully developed telencephalon from both the diencephalon and mesencephalon.
The transverse fissure has two parts:
(A) A median portion located between the telencephalic commissures (corpus callosum and fornix) above and the diencephalon below the cistern of the velum interpositum, and
(B) Paired right and left lateral portions surrounding the mesencephalon (Figs. 1.3 and 1.30).

B. Brain stem surface

Each of the three segments of the brain stem presents anterior, posterior and lateral aspects, which will be described in turn (see [48, 78, 85, 99, 109, 167, 228, 250, 251, 273, 322, 324, 334, 357, 387, 430, 445, 455]).

Figure 1.4 displays the anterior surface of the brain stem including the medullary pyramids, the belly of the pons, the cerebral peduncles, and the origins of all the cranial nerves, except the trochlear (CN IV).

Figure 1.5 displays the posterior surface of the brain stem including the characteristic shape of the fourth ventricle (rhomboid fossa), the surface features of the fourth ventricular floor, the structures of the quadrigeminal plate, and the origin of the trochlear nerve (CN IV).

Figure 1.6 displays the lateral aspect of the brain stem including the relative ventral-dorsal positions of the cranial nerve origins, the dorsally converging angulations of the three cerebellar peduncles, and the relationships among the inferior colliculus, its brachium and the medial geniculate body.

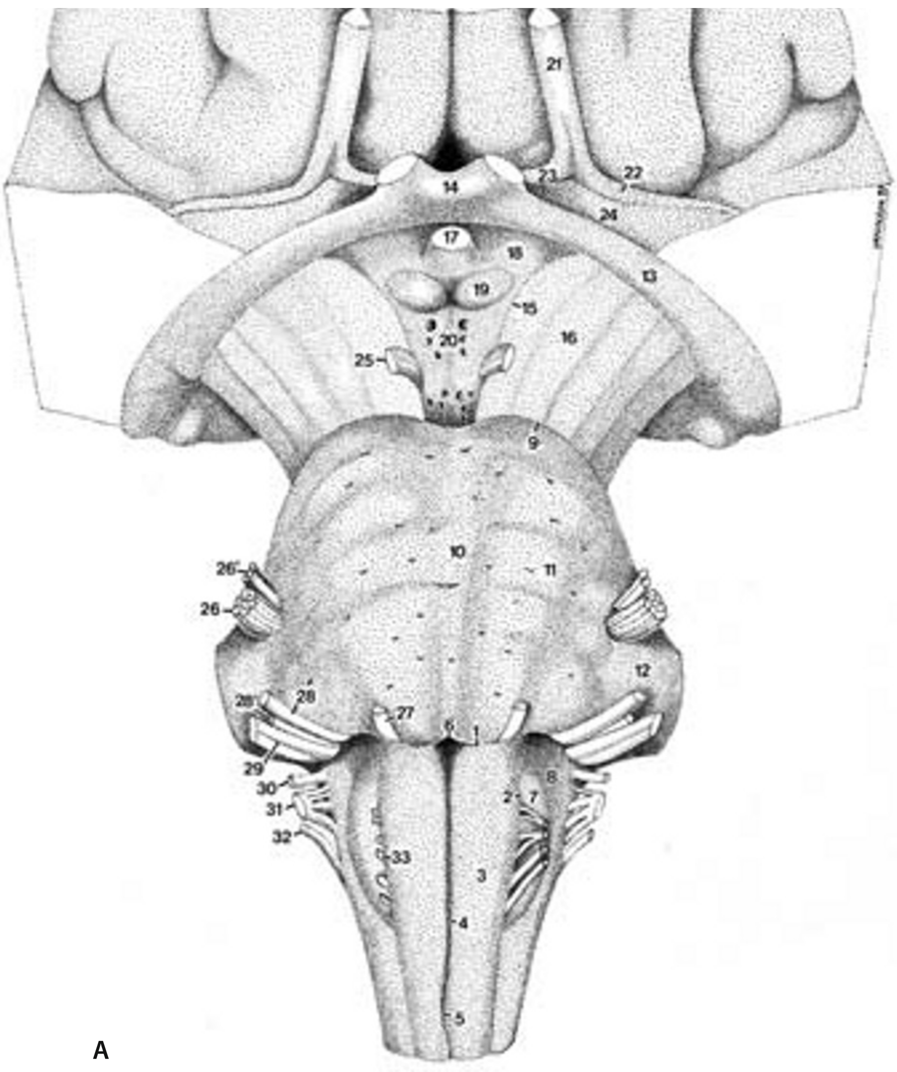

A

Fig. 1.4 (A–B). The brain stem. Anterior view. Bar: 5 mm.

Medulla

The boundaries between the spinal cord and medulla are noted on **Fig. 1.30.** The pontomedullary sulcus (1) separates the medulla from the pons.

Anterior aspect

1 Pontomedullary sulcus
2 Anterolateral medullary (pre-olivary) sulcus
3 Pyramid of the medulla (including corticospinal tract)
4 Anterior median medullary sulcus
5 Pyramidal decussation (spinomedullary junction)
6 Foramen cecum

Lateral aspect

7 Inferior olive
8 Lateral fossa of the medulla

Pons

The pons is separated from the medulla by the pontomedullary sulcus (1) and from the mesencephalon by the pontomesencephalic sulcus (9).

Anterior aspect

9 Pontomesencephalic sulcus
10 Basilar sulcus
11 Basilar (ventral) portion of the pons

The lateral aspect of the pons (12) merges into the middle cerebellar peduncle (brachium pontis).

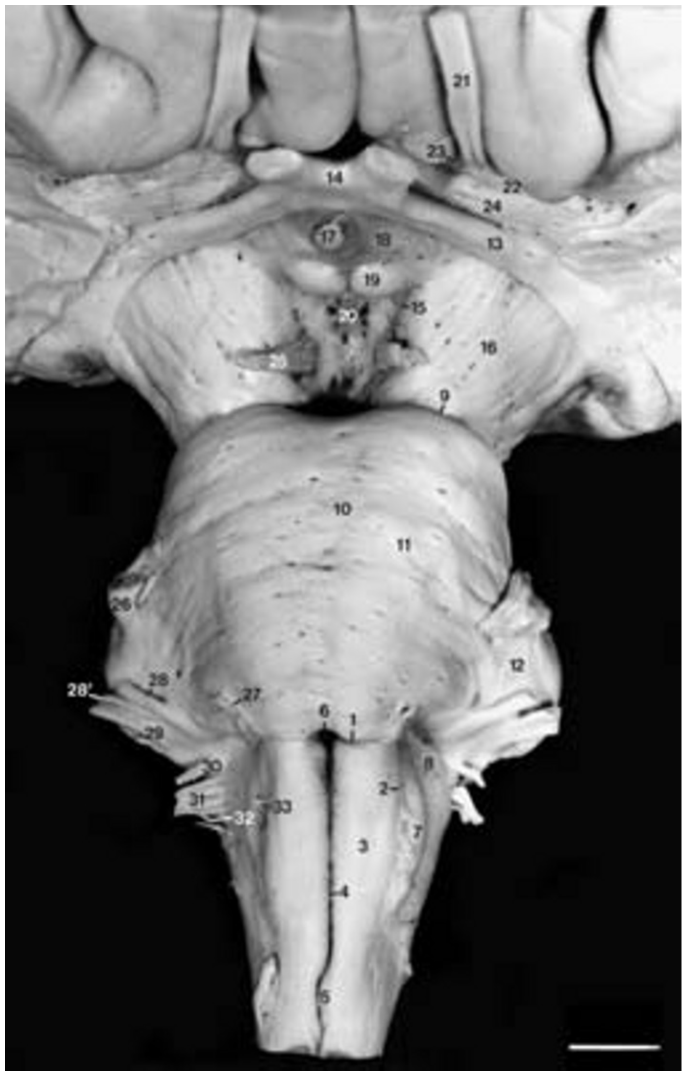

B

Mesencephalon
The mesencephalon is separated from the pons by the pontomesencephalic sulcus (9) and from the brain by the optic tract (13), the optic chiasm (14), and the medial mesencephalic sulcus (15).

Anterior aspect
The mesencephalon consists of the crus cerebri (pes pedunculi or basis pedunculi) (16).

The interpeduncular region, which belongs to the diencephalon, includes the hypophyseal stalk (17), tuber cinereum (18), mammillary bodies (19), and interpeduncular fossa (posterior perforated substance) (20).

Also shown are the olfactory tracts (21), dividing into lateral (22) and medial (23) olfactory striae bordering the anterior perforated substance (24).

Roots of the cranial nerves
25 Oculomotor nerve
26 Trigeminal nerve (sensory root)
26′ Trigeminal nerve (motor root)
27 Abducens nerve
28 Facial nerve
28′ Nervus intermedius
29 Vestibulocochlear nerve
30 Glossopharyngeal nerve
31 Vagus nerve
32 Accessory nerve (medullary root)
33 Hypoglossal nerve

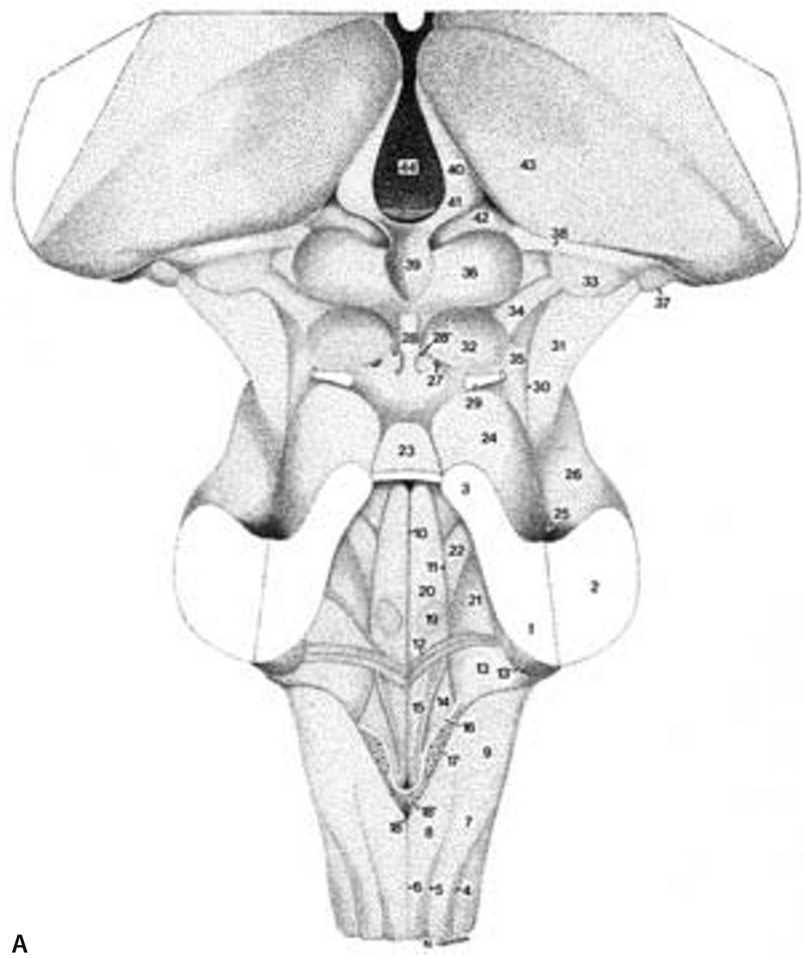

A

Fig. 1.5 (A–B). The brain stem. Posterior view. The cerebellum was removed by section of the three cerebellar peduncles: inferior (restiform body) (1), middle (brachium pontis) (2), and superior (brachium conjunctivum) (3). Bar: 5 mm.

Medulla – posterior aspect

The medulla is divided into superior and inferior levels. The superior level belongs to the floor of the fourth ventricle. The inferior level extends to the posterior aspect of the spinal cord.

Inferior level

4 Posterolateral medullary sulcus
5 Posterior intermediate medullary sulcus
6 Posterior median medullary sulcus

The cuneate tubercle (7) and gracile tubercle (clava) (8) are produced by the subjacent cuneate and gracile nuclei (See Fig. 2.8).

Superior level

The superior level is composed of the medullary portion of the fourth ventricular floor and the right and left inferior cerebellar peduncles (9).

Pons – posterior aspect

This aspect of the pons mostly consists of the pontine (superior) portion of the fourth ventricular floor.

Floor of the fourth ventricle (Rhomboid fossa)

The floor or rhomboid fossa (See Fig. 2.6) shows one median sulcus (10) and paired right and left paramedian sulci limitantes (11). The striae medullares (12) divide the floor into the inferior medullary triangle and superior pontine triangle.

Brain stem surface

The medullary triangle consists of three segments (13, 14 and 15) that run from the lateral region to the median line.

13 Medullary vestibular area (due to the protrusion of the medial vestibular nucleus);
13′ Acoustic tubercle
14 Vagal trigone (fovea inferior) corresponding to the dorsal motor nucleus of the vagus
15 Hypoglossal trigone produced by the subjacent hypoglossal and intercalated nuclei.
16, 17 A thickening of the ependyma, the funiculus separans (16), borders the area postrema (17) (See Fig. 1.21).
18 Obex
18′ Funicular commissure linking the right and left funiculi separantes (16) (See Fig. 1.21).

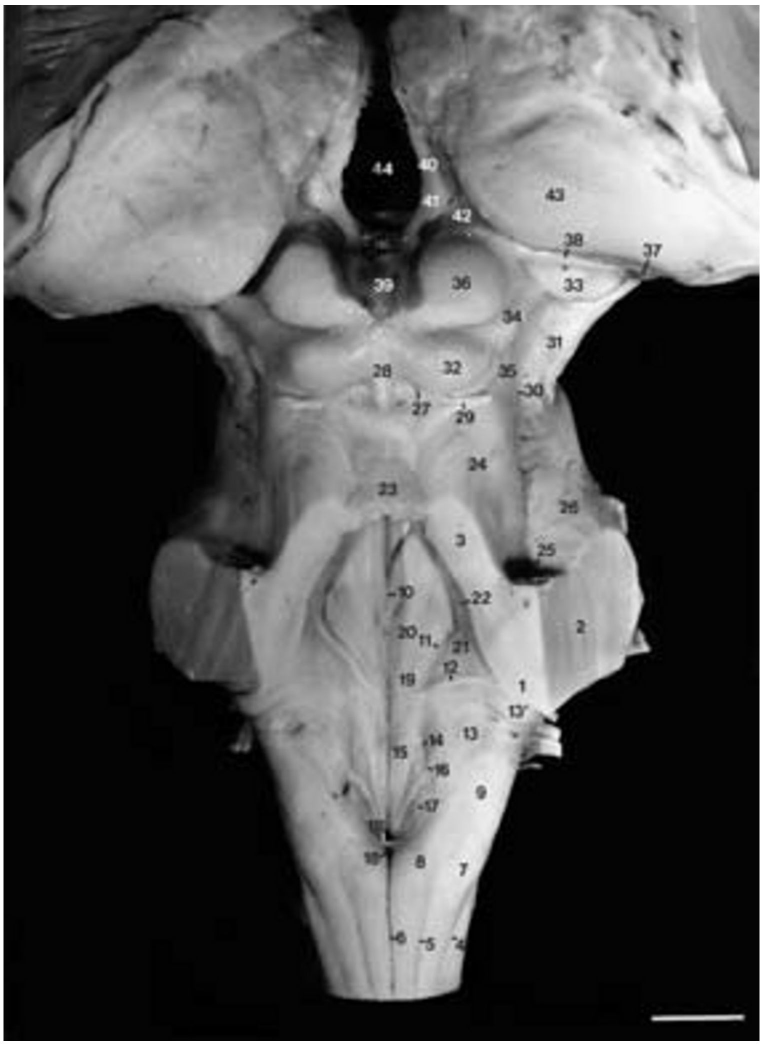

B

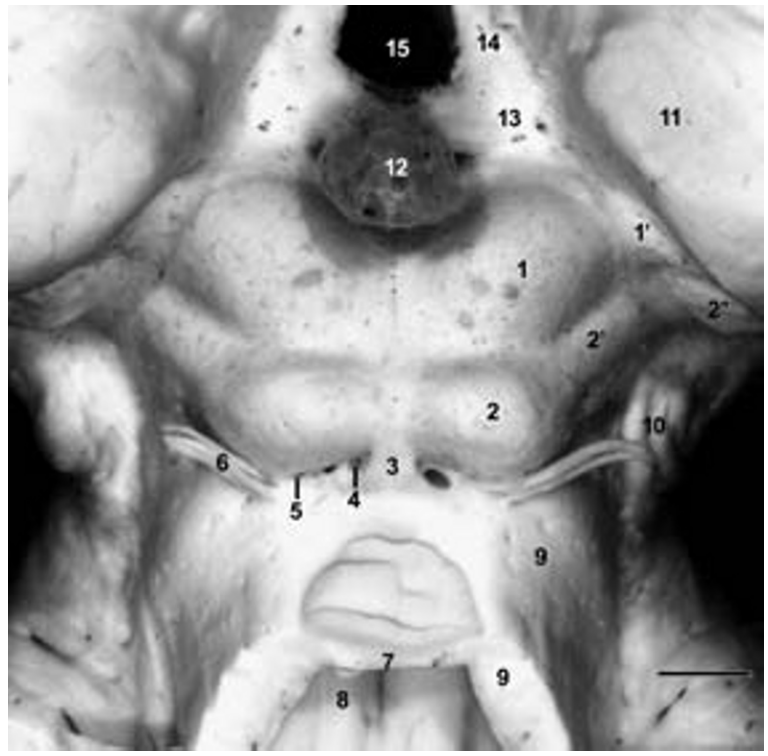

C

The pontine triangle consists of

19 Facial colliculus (protrusion due to the abducens nucleus- and the facial nerve fibers)
20 Medial eminence
21 Pontine vestibular area
22 Superior fovea (fovea trigemini)
23 Superior medullary velum linking the right and left superior cerebellar peduncles (brachia conjunctiva) (24).
25 Parabrachial recess (**See Figs. 11.18 and 11.19**) situated between the brachium conjunctivum (24) and the brachium pontis (26)

Mesencephalon - posterior and lateral aspects

27 Infracollicular recess (emergence of deep veins **[122]**)
28 Frenulum veli
29 Root of the trochlear nerve
30 Lateral mesencephalic sulcus bordering the crus cerebri (31)
32 Inferior colliculus linked to the medial geniculate body (33) by the brachium of the inferior colliculus (34)
35 Lateral aspect of mesencephalon
36 Superior colliculus linked to the lateral geniculate body (37) by the brachium of the superior colliculus (38)
39 Pineal gland
40 Stria medullaris thalami
41 Habenular trigone
42 Pretectal area
43 Thalamus (pulvinar)
44 Third ventricle

C. The mesencephalon. Enlarged posterior view. Bar: 5 mm.

1 Superior colliculus
1′ Brachium of the superior colliculus
2 Inferior colliculus
2′ Brachium of the inferior colliculus
2″ Medial geniculate body
3 Frenulum veli
4 Recess of the frenulum veli
5 Infracollicular recess
6 Root of the trochlear nerve
7 Superior medullary velum
8 Fourth ventricle
9 Superior cerebellar peduncle (brachium conjunctivum)
10 Crus cerebri (cerebral peduncle)
11 Pulvinar
12 Pineal gland
13 Habenular trigone (site of medial and lateral habenular nuclei)
14 Stria medullaris thalami
15 Third ventricle

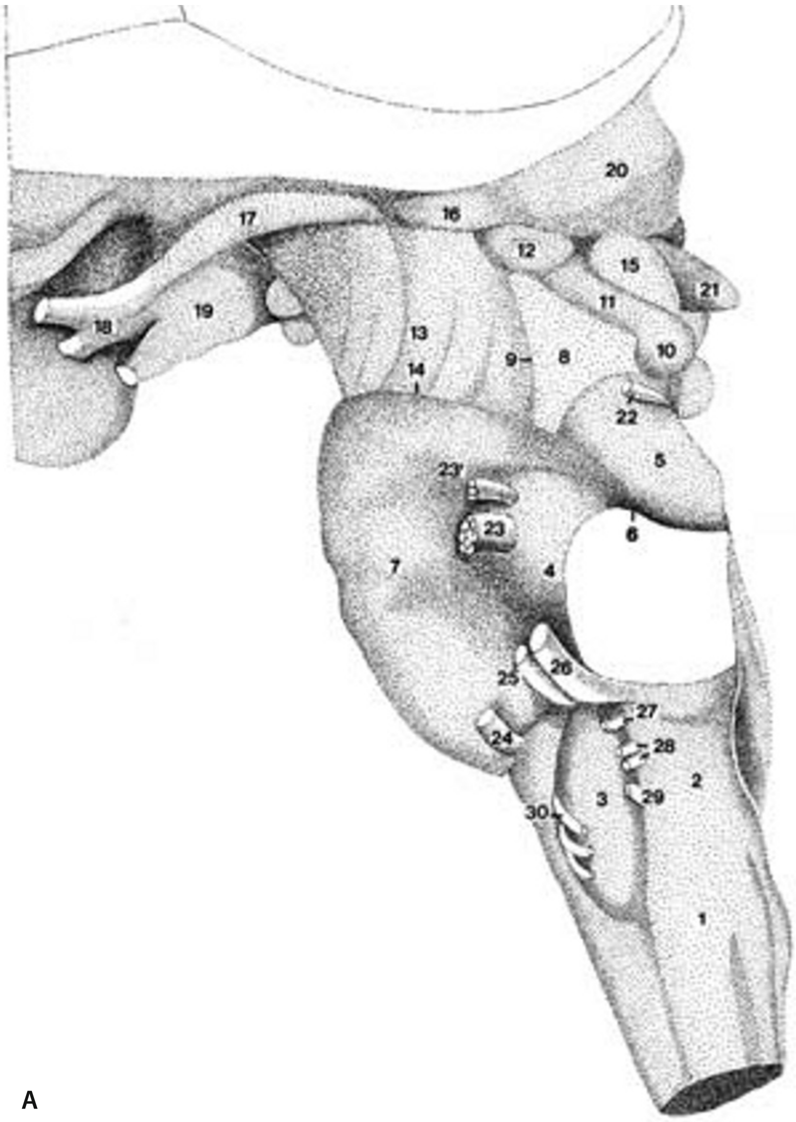

A

Fig. 1.6 (A–B). The brain stem. Lateral view.
Bar: 5 mm.

Medulla – lateral aspect
Inferior level
1 Lateral medullary funiculus

Superior level
2 Inferior cerebellar peduncle (restiform body)
3 Inferior olive

Pons – lateral aspect
The lateral aspect of the pons is formed by the middle cerebellar peduncle (brachium pontis) (4)
5 Superior cerebellar peduncle (brachium conjunctivum)
6 Parabrachial recess
7 Anterior aspect of the pons

Mesencephalon – lateral aspect
This lateral surface is also called the acoustic or lemniscal trigone due to the underlying lateral lemniscus (auditory fibers).

B

The triangular lateral aspect of the mesencephalon (8) is bordered laterally by the mesencephalic sulcus (9), posteriorly by the inferior colliculus (10) and its brachium (11), cranially by the medial geniculate body (12), and caudally by the superior cerebellar peduncle (5) (brachium conjunctivum).

13 Crus cerebri
14 Pontomesencephalic sulcus
15 Superior colliculus
16 Lateral geniculate body
17 Optic tract
18 Optic chiasm
19 Median eminence of the tuber cinereum
20 Pulvinar
21 Pineal gland

Roots of cranial nerves
22 Trochlear nerve
23 Trigeminal nerve, sensory root
23′ Trigeminal nerve, motor root
24 Abducens nerve
25 Facial nerve
26 Vestibulocochlear nerve
27 Glossopharyngeal nerve
28 Vagus nerve
29 Accessory nerve (medullary root)
30 Hypoglossal nerve

C. Cerebellar surface

The cerebellum consists of the median vermis and the paired left and right cerebellar hemispheres. The superior vermis rises above the cerebellar hemispheres, while the inferior vermis is deeply embedded between the two cerebellar hemispheres, within the posterior cerebellar notch and vallecula.

The cortex covering the cerebellum is tightly folded. A single fold is called a folium. Multiple folds are called folia; grouped folia form lobules that are separated by fissures. Each lobule has a median portion belonging to the vermis and paired lateral portions belonging to the two cerebellar hemispheres.

The lobules group together into anterior, posterior, and flocculonodular cerebellar lobes. The anterior lobe is separated from the posterior lobe by the primary fissure. The posterior lobe is separated from the flocculonodular lobe by the posterolateral fissure (**Fig. 1.7**).

Figure 1.7 depicts the cerebellar anatomy as seen from the midline. Figure 1.8 diagrams the cerebellar surface as if it were unrolled and seen, simultaneously, from the ventral, superior, and inferior perspectives (**See arrows in Fig. 1.7**). Table 1.1 summarizes the relationships among the lobules and fissures of the vermis and cerebellum. Figures 1.9 through 1.17 then depict the surface anatomy of the cerebellum. See [15, 48, 55, 61, 78, 85, 92, 99, 109, 155, 167, 218, 228, 248, 251, 253, 254, 255, 273, 322, 324, 334, 342, 343, 350, 357, 387, 430, 445, 474, 475, 476].

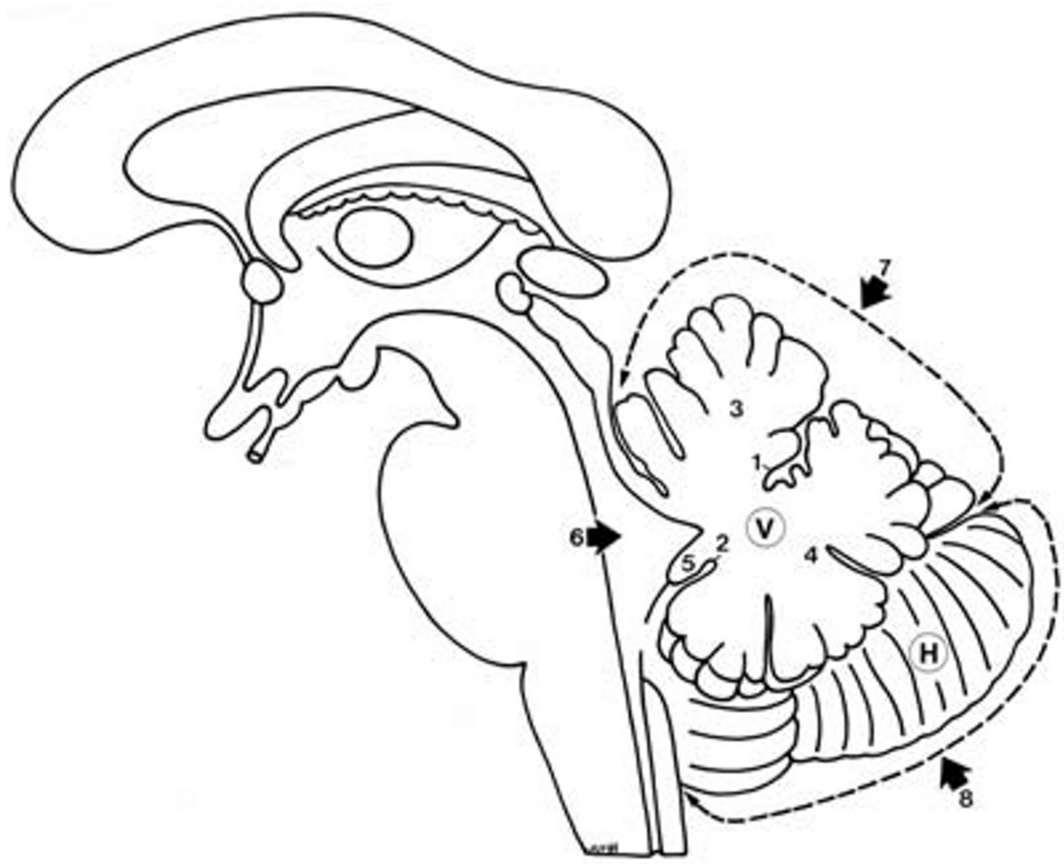

Fig. 1.7. Diagram. Median section of the vermis (V) and medial surface of the cerebellar hemisphere (H).

1 Anterior superior fissure (primary fissure)
2 Posterolateral fissure
3 Anterior lobe
4 Posterior lobe
5 Flocculonodular lobe
6 Viewpoint for the anterior aspect of the cerebellum
7 Viewpoint for the superior aspect
8 Viewpoint for the inferior aspect

The dotted line indicates the superior and inferior aspects of the cerebellum as shown in Fig. 1.8.

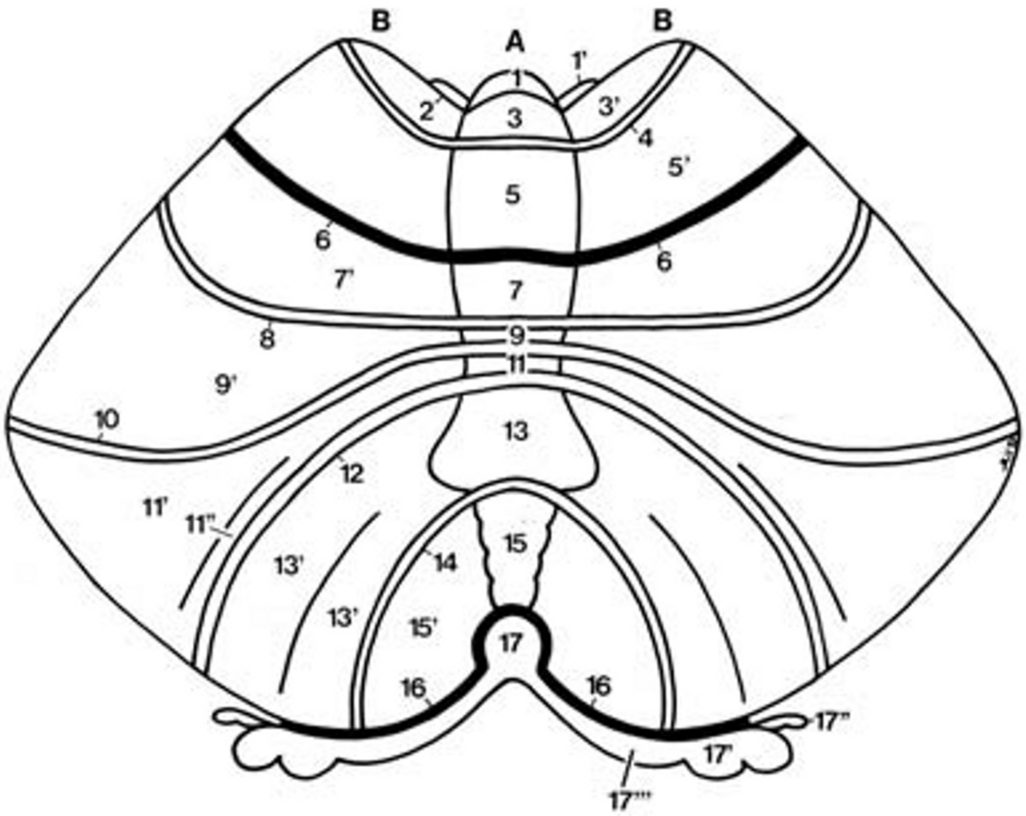

Fig. 1.8. The unrolled surface of the cerebellum. Composite diagram, as seen from the viewpoints shown in Fig. 1.7.
A. Vermis, **B.** Cerebellar hemispheres. The terminology used to describe the cerebellum is particularly complex. This book tries to use the most common terms (and provides synonyms in brackets for comparison with other texts) [218, 255].

I. Anterior lobe

- 1 Lingula (**lobule I** of Jansen, only applied to the vermis)
- 1′ Vinculum lingulae (likely vestigial in man)
- 2 Precentral fissure
- 3 Central lobule (**lobules II and III** of Jansen)
- 3′ Wing of the central lobule
- 4 Preculminate fissure (postcentral fissure)
- 5 Culmen (**lobules IV and V**)
- 5′ Quadrangular lobule (anterior quadrangular lobule)
- 6 Anterior superior fissure (primary fissure)

II. Posterior lobe

- 7 Declive (**lobule VI**)
- 7′ Simple lobule (posterior quadrangular lobule)
- 8 Posterior superior fissure (postclival fissure)
- 9 Folium (**lobule VII** of Jansen)
- 9′ Superior semilunar lobule (crus I)
- 10 Great horizontal fissure (intercrural fissure)
- 11 Tuber (**also lobule VII** of Jansen)
- 11′ Inferior semilunar lobule (crus II). The superior and inferior semilunar lobules (crura I and II) together form the ansiform lobule.
- 11″ Gracile lobule (paramedian lobule). This is sometimes considered to belong to the inferior semilunar lobule, but may be separated from the latter by the ansoparamedian fissure.
- 12. Prepyramidal fissure. For simplicity, this term is sometimes used for both the vermian and the hemispheric portions of the fissure.
- 13 Pyramis (pyramid) of the vermis (**lobule VIII** of Jansen)
- 13′ Biventral lobule (digastric lobule, dorsal paraflocculus) divided into two portions by the intrabiventral fissure
- 14 Postpyramidal fissure (secondary fissure). For simplicity, this term may also be used for both the vermian and the hemispheric portions of the fissure.
- 15 Uvula (**lobule IX** of Jansen)
- 15′ Tonsil (cerebellar amygdala, ventral paraflocculus)
- 16 Posterolateral fissure (postnodular fissure)

III. Flocculonodular lobe

- 17 Nodulus (**lobule X**)
- 17′ Flocculus
- 17″ Paraflocculus (accessory paraflocculus)
- 17‴ Floccular brachium (floccular peduncle)

Table 1.1. Lobes, lobules and fissures of the cerebellum

Classical 3 Lobes	Yasargil[476] 4 Lobes	Larsell[253-255] 10 Divisions	Vermis 9 Lobules	Hemispheres 10 Lobules	Intervening Fissure 10 Fissures
Anterior Medullary Velum					
		I	Lingula	Vinculum	
					Precentral Fissure
Anterior Lobe	Anterior Lobe	II, III	Central	Wing of Central	
					Preculminate Fissure
		IV, V	Culmen	Anterior Quadrangular	
					Primary Fissure
		VI	Declive	Lobulus Simplex	
	Middle Lobe				Posterior Superior Fissure
		VII	Folium	Superior Semilunar	
					Great Horizontal Fissure
		VII	Tuber	Inferior Semilunar	
					Fissura Ansoparamedianus
Posterior Lobe			Prepyramidal Fissure	Lobulus Gracilis	
					Prebiventral Fissure
	Posterior Lobe			Biventral Lobule	
		VIII	Pyramis		Intrabiventral Fissure
				Biventral Lobule	
					Secondary Fissure
		IX	Uvula	Tonsil	
					Posterolateral Fissure
Flocculo-Nodular Lobe	Flocculo-Nodular Lobe	X	Nodulus	Flocculus	
Posterior Medullary Velum					

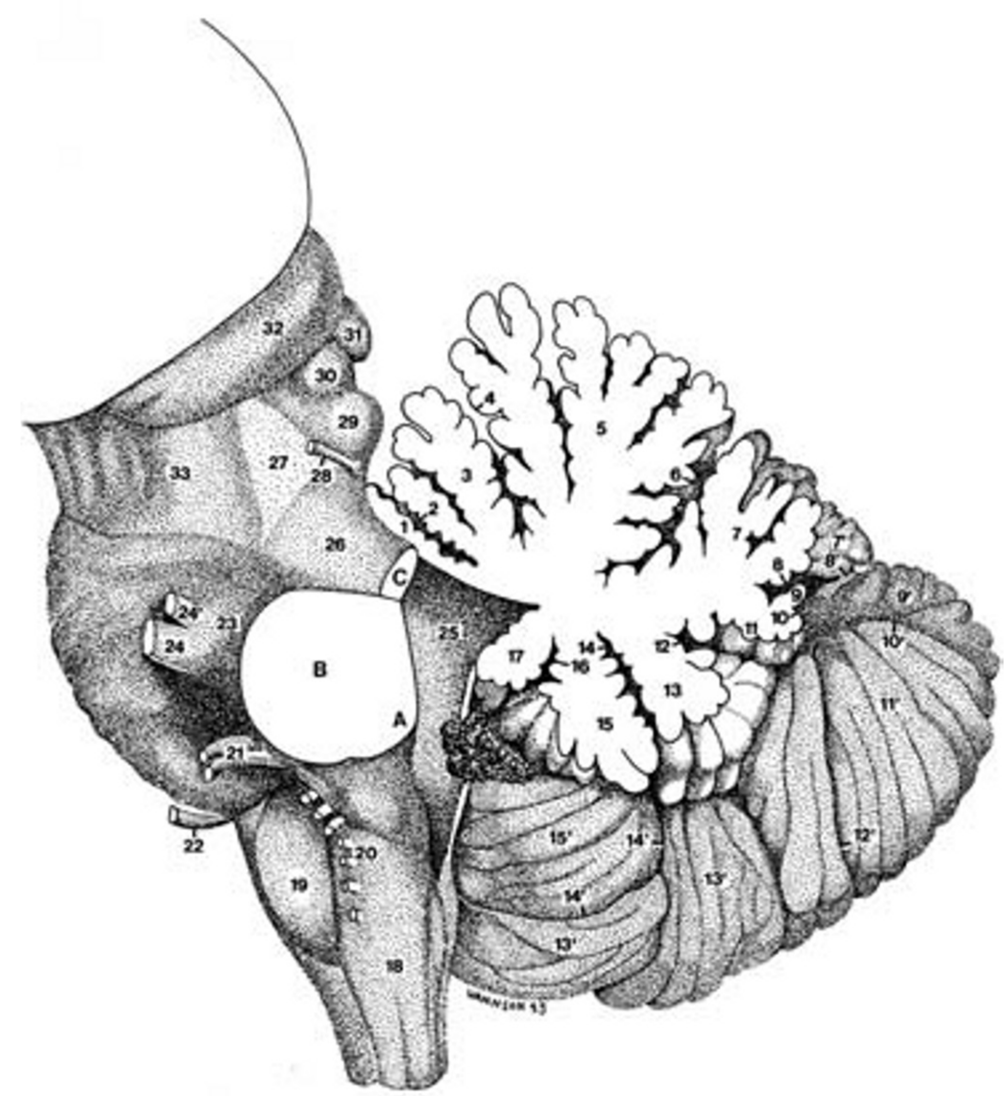

A

Fig. 1.9 (A–B). The vermis. Median section. Diagram **(A)** and specimen photograph **(B)** display the medial view of the cerebellar hemisphere and the lateral view of the brain stem. The inferior (A), middle (B), and superior (C) cerebellar peduncles have been resected. Bar: 5 mm.

Median section of the vermis

1 Lingula
2 Precentral fissure
3 Central lobule
4 Preculminate fissure
5 Culmen
6 Anterior superior fissure (primary fissure)
7 Declive
8 Posterior superior fissure
9 Folium
10 Great horizontal fissure (the vermian portion of the horizontal fissure is difficult to identify)
11 Tuber
12 Prepyramidal fissure
13 Pyramid of the vermis (pyramis)
14 Postpyramidal fissure (secondary fissure)
15 Uvula
16 Posterolateral fissure
17 Nodulus

Medial view of the left cerebellar hemisphere

7′ Simple lobule
8′ Posterior superior fissure
9′ Superior semilunar lobule
10′ Horizontal fissure
11′ Inferior semilunar lobule
12′ Prepyramidal fissure
13′ Biventral lobule
14′ Postpyramidal fissure
15′ Tonsil

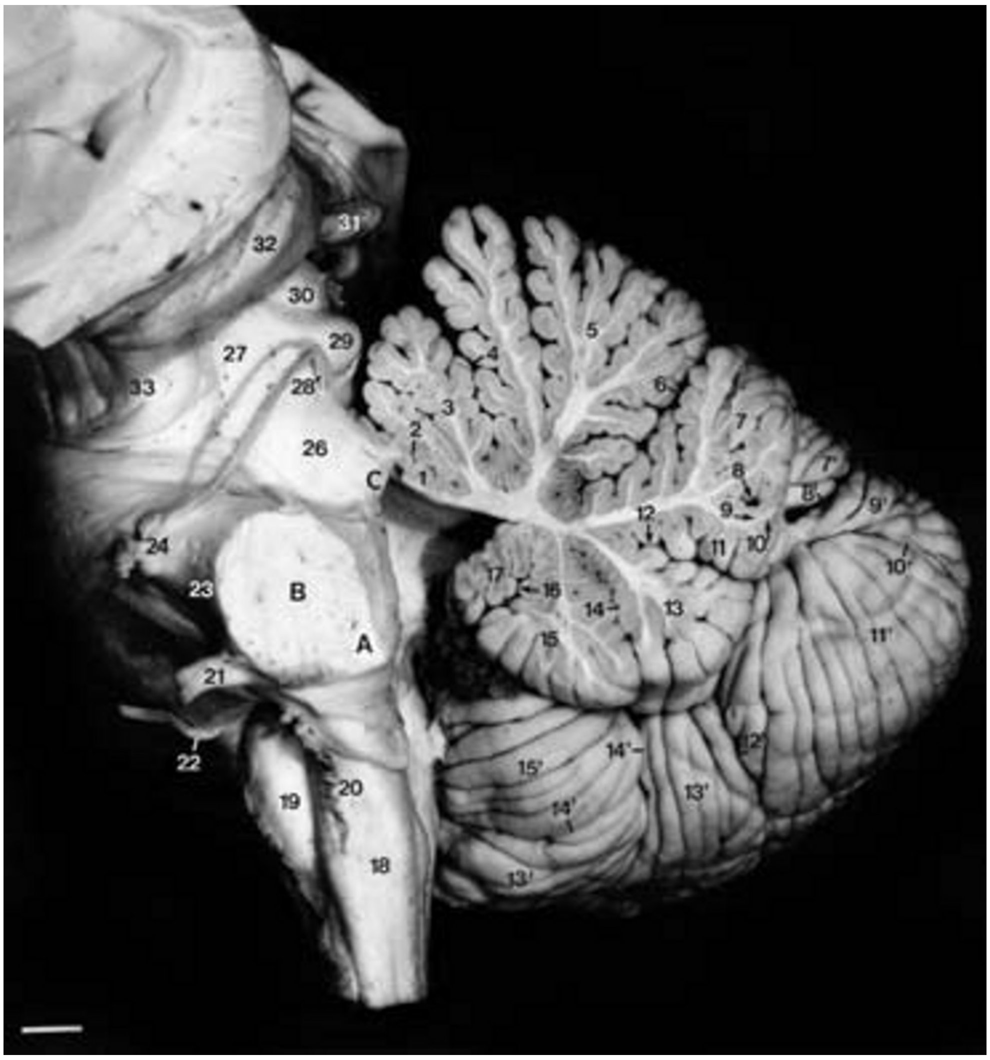

B

Lateral view of the brain stem

18 Lateral aspect of the medulla
19 Inferior olive
20 Roots of glossopharyngeal, vagus, and accessory nerves, in descending order
21 Roots of vestibulocochlear and facial nerves
22 Root of abducens nerve
23 Lateral aspect of the pons (middle cerebellar peduncle)
24 Sensory root of trigeminal nerve
24′ Motor root of trigeminal nerve
25 Fourth ventricle
26 Superior cerebellar peduncle (brachium conjunctivum)
27 Lateral aspect of the mesencephalon
28 Trochlear nerve
29 Inferior colliculus
30 Superior colliculus
31 Pineal gland
32 Pulvinar
33 Crus cerebri